RESEARCH ARTICLE | MAY 23 2025

Non-Abelian Thouless pumping in a Rice–Mele ladder

Carlo Danieli ; Valentina Brosco ; Laura Pilozzi ; Roberta Citro

AVS Quantum Sci. 7, 022001 (2025)
https://doi.org/10.1116/5.0245350

Non-Abelian Thouless pumping in a Rice–Mele ladder

Cite as: AVS Quantum Sci. 7, 022001 (2025); doi: 10.1116/5.0245350
Submitted: 25 October 2024 · Accepted: 19 February 2025 ·
Published Online: 23 May 2025

Carlo Danieli,[1,a] Valentina Brosco,[1,2,b] Laura Pilozzi,[1,3] and Roberta Citro[4,5]

AFFILIATIONS

[1]Istituto dei Sistemi Complessi, Consiglio Nazionale delle Ricerche, Via dei Taurini 19, 00185 Rome, Italy
[2]Dipartimento di Fisica, Università "La Sapienza," P.le A. Moro, 5 (00185) Roma, Italy
[3]Centro Ricerche Enrico Fermi, Piazza del Viminale, 1, I-00184 Rome, Italy
[4]Dipartimento di Fisica "E.R. Caianiello," Università di Salerno, Via Giovanni Paolo II, 132, I-84084 Fisciano (SA), Italy
[5]CNR-SPIN, c/o Università di Salerno, Via Giovanni Paolo II, 132, I-84084 Fisciano (SA), Italy

[a)]Electronic mail: carlo.danieli@cnr.it
[b)]Electronic mail: valentina.brosco@cnr.it

ABSTRACT

Non-Abelian Thouless pumping intertwines adiabatic quantum control and topological quantum transport, and it holds potential for quantum metrology and computing. In this work, we introduce a ladder model featuring two doubly degenerate bands and we show that adiabatic manipulation of the lattice parameters results in non-Abelian Thouless pumping, inducing both the displacement of an initially localized state and a geometric unitary transformation within the degenerate subspace. Additionally, we show that the structure and symmetry of the ladder model can be understood through its connection to a Yang monopole model. The proposed Hamiltonian can be realized using cold atoms in optical lattices, enabling the experimental demonstration of non-Abelian Thouless pumping in a genuinely quantum many-body system.

I. INTRODUCTION

An important geometric aspect of quantum mechanics emerges when the Hamiltonian of a quantum system varies adiabatically and cyclically with time. In this case, the evolution operator over a cycle yields a transformation that depends solely on the topological structure of the Hilbert space and the geometry of the cycle while being independent of dynamical details such as the energy levels or the cycle duration. When the adiabatic evolution involves a non-degenerate eigenstate the geometric part of the evolution coincides with the Berry's phase,[1] conversely, for a N-degenerate eigenstate the geometric evolution is a $U(N)$ transformation, called non-Abelian holonomy.[2] Beyond their significance in adiabatic quantum evolution, geometric phases and holonomies are crucial for understanding the properties of Bloch bands in solids[3] and underlie polarization theory and many fascinating phenomena, such as quantum Hall effect,[4] the spin Hall effect,[5] and topological phases.[6]

The interplay of geometry, lattice symmetries, and adiabatic dynamics emerges in particular in Thouless pumping.[7] Thouless pumping refers to transport induced by the adiabatic and cyclic manipulation of a lattice potential in the absence of any external bias. Under suitable conditions, this phenomenon yields topologically quantized transport, enabling the direct measurement of topological invariants.[7] Thouless pumping has been experimentally realized in various systems,[8] including cold atoms and spin in optical lattices,[9–11] and photonic waveguide arrays.[12] It can be employed to explore the breakdown of topological phenomena in the presence of interactions,[13–18] disorder,[19,20] non-linearities,[21,22] or dissipation.[23] In these situations, it can give rise fractional topological quantization[21,24–27] and topological phase transitions. Recent theoretical work[28] has demonstrated that Thouless pumping can exhibit non-Abelian characteristics in systems with degenerate Bloch bands. Subsequently, non-Abelian Thouless pumping has been implemented in photonic[29,30] and acoustic waveguide arrays.[31] In these setups, the propagation of electromagnetic waves is effectively described by an Hamiltonian having a tripod structure[28,32] and featuring a doubly degenerate flat band. Tripod Hamiltonians have long been studied in relation to non-Abelian holonomies in atomic transitions,[33] superconducting nanocircuits,[34] Cooper pair pumps,[35] and more recently photonic systems.[36]

In the present work, we envisage a non-Abelian Thouless pump in a lattice with two dispersive, doubly degenerate bands—hence moving beyond the paradigm of tripod flat-band systems discussed in Ref. 28. The Hamiltonian has a ladder structure and can be implemented with cold atoms in optical lattices, thereby enabling the demonstration of non-Abelian Thouless pumping in an inherently quantum many-body system. Furthermore, as we show below, its structure and symmetry properties[37] can be explained through a relation with a Yang monopole model.[38,39] Thanks to their exceptionally high level of control and robustness, non-Abelian Thouless pumps hold significant promise for applications in quantum computing,[40,41] routing,[42] and metrology.[43–45] Our work therefore has both a practical and fundamental relevance as it paves to the development of different holonomic devices and the investigation of the interplay between the geometric and dynamical properties of many-body quantum systems.

II. RICE–MELE LADDER

The Hamiltonian describes two coupled Rice–Mele[46] chains, and it can be cast as follows:

$$H = \sum_n \sum_{M=U,D} \left[J_1\, a^\dagger_{n,M} b_{n,M} + J_2\, a^\dagger_{n,M} b_{n-1,M} + \text{H.c.} \right] + \mu \sum_n \left[a^\dagger_{n,U} a_{n,U} - a^\dagger_{n,D} a_{n,D} - b^\dagger_{n,U} b_{n,U} + b^\dagger_{n,D} b_{n,D} \right] + \rho \sum_n \left[a^\dagger_{n,U} a_{n,D} - b^\dagger_{n,U} b_{n,D} + \text{H.c.} \right], \quad (1)$$

where $c^\dagger_{n,M}$ and $c_{n,M}$ (with $c = a, b$) are the creation and annihilation operators of sublattice a, b in the unit cell n and chain $M = U, D$. In Eq. (1), J_1 and J_2 represent the intra- and inter-cell hopping along the two chains, μ is a staggered on-site potential, and ρ is a staggered interchain coupling. The model is schematically illustrated in Fig. 1(a).

Introducing the four-dimensional spinor creation and annihilation operator $\Psi^\dagger_k = (a^\dagger_{k,U}, a^\dagger_{k,D}, b^\dagger_{k,U}, b^\dagger_{k,D})$, we can recast the Hamiltonian H in momentum space as

$$H = \sum_k \Psi^\dagger_k \left[(J_x \tau_x + J_y \tau_y) \otimes \sigma_0 + \tau_z \otimes (\rho\, \sigma_x + \mu\, \sigma_z) \right] \Psi_k. \quad (2)$$

Here, $J_k = J_1 + J_2 e^{ik}$ is decomposed as the sum of $J_x = J_1 + J_2 \cos k$ and $J_y = J_2 \sin k$ and σ_j and τ_j are Pauli matrices spanning the spin and site indices. The Bloch spectrum of the ladder consists of two doubly degenerate bands with dispersion

$$E_\pm(k) = \pm \sqrt{\mu^2 + \rho^2 + |J_k|^2} \equiv \pm \Delta, \quad (3)$$

shown in Fig. 1 for $\mu \equiv 0$ and $\rho \equiv 0$ corresponding to the Bloch states (see the supplementary material for details)

$$|\psi^\pm_a(k)\rangle = \frac{1}{\mathscr{R}_\pm} \left[\rho |a_{k,U}\rangle + (-\mu \pm \Delta) |a_{k,D}\rangle + J_k |b_{k,D}\rangle \right], \quad (4)$$

$$|\psi^\pm_b(k)\rangle = \frac{1}{\mathscr{R}_\pm} \left[-J^*_k |a_{k,U}\rangle + (\mu \mp \Delta) |b_{k,U}\rangle + \rho |b_{k,D}\rangle \right], \quad (5)$$

so that $H|\psi^\pm_m(k)\rangle = E_\pm(k)|\psi^\pm_m(k)\rangle$ with $m = a, b$ and $\mathscr{R}_\pm = \sqrt{2\Delta(\Delta \mp \mu)}$. The spectrum is thus gapless for $\mu = \rho = 0$ and $J_1 = J_2$ and gapped otherwise.

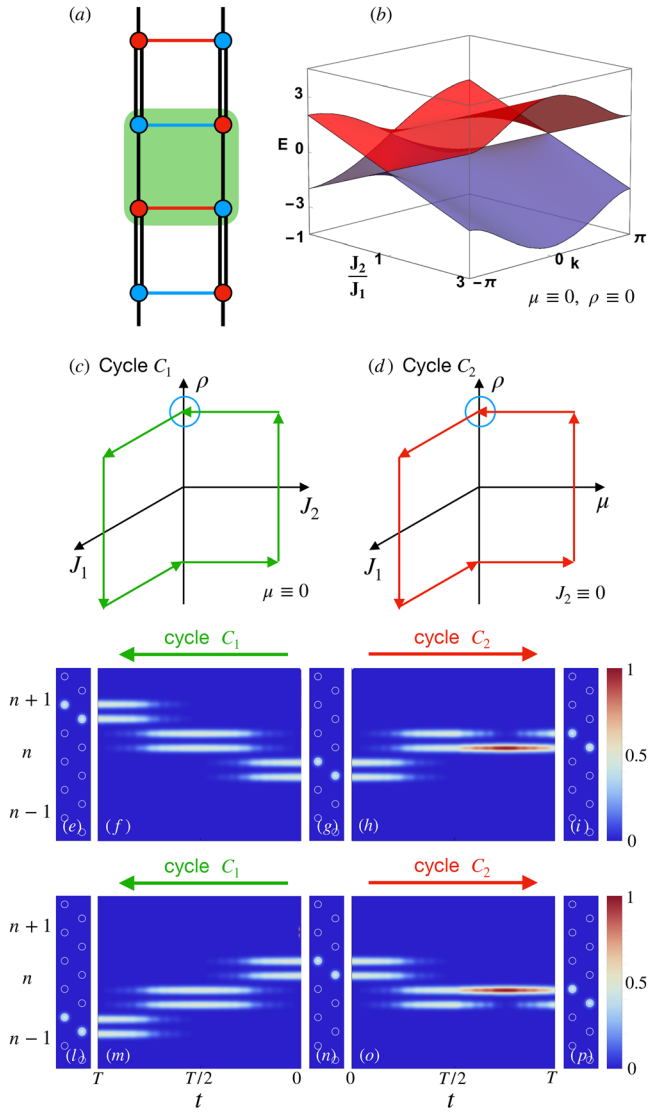

FIG. 1. (a) Rice–Mele ladder describing two coupled Rice–Mele chains red and blue colors indicate opposite on-site potential or interchain tunneling. (b) Bloch bands vs J_2/J_1 for $\mu \equiv 0$ and $\rho \equiv 0$. (c) and (d) Pumping cycles C_1 and C_2. The blue circles indicate the initial point. Panels (e)–(p) display the field's intensity along C_1 and C_2 with initial state $|v^+_{a,n_0}\rangle$ (e)–(i) and initial state v^-_{a,n_0} (l)–(p).

III. NON-ABELIAN THOULESS PUMPING

Thouless pumping is achieved by modulating periodically and adiabatically at least two parameters defining the Hamiltonian H. The non-Abelian nature of the evolution implies that pumping cycles can not only shift but also geometrically manipulate bond and plaquette states along the ladder. At time $t = 0$, we initialize the system in a Wannier state defined as $|\psi^\pm_{n_0}(0)\rangle = \sum_{k,\nu} c_\nu |\psi^\pm_\nu(k)\rangle e^{ikn_0}$ belonging to one of the two bands $E_\pm$ and localized within the unit cell n_0. Following Ref. 28, in the adiabatic regime, the evolution of $|\psi^\pm_{n_0}(0)\rangle$ can be expressed as follows:

$$|\psi^{\pm}_{n_0}(T)\rangle = \sum_{k\nu\eta} c_\nu \left[W^{\pm}(0,T)\right]_{\eta\nu} |\psi^{\pm}_{\eta}(k)\rangle e^{ikn_0}, \tag{6}$$

where T denotes the driving period and the adiabatic evolution operator is given by[28]

$$W_{\pm}(0,T) = e^{i\theta^{\pm}_{\mathrm{d}}} \mathscr{P} \exp\left[i\int_0^T \Gamma^{\pm}_t dt\right]. \tag{7}$$

In the above equation, $\theta^{\pm}_{\mathrm{d}}$ denotes the dynamical phase $\theta^{\pm}_{\mathrm{d}} = \int_0^T E_{\pm}(t)dt$, while the geometric part of $W_{\pm}$ is given by a path ordered exponential $\mathscr{P}$ of the Wilczek–Zee connection $[\Gamma^{\pm}_t]_{\nu\nu'} = \langle\psi^{\pm}_{\nu}(k)|i\partial_t|\psi^{\pm}_{\nu'}(k)\rangle$ associated with the two bands.[2]

Starting from Eqs. (4) and (5), we can express the connection $\Gamma^{\pm}_t$ generated by time-dependent drivings on the different parameters of the Hamiltonian H as follows:

$$\Gamma^{\pm}_t = \frac{1}{\mathscr{R}^2_{\pm}}\Big[\left(J_2\dot{J}_1 - J_1\dot{J}_2\right)\sin k\,\hat{\sigma}_z + \left(\dot{J}_1\rho - J_1\dot{\rho}\right)\hat{\sigma}_y + \left(\dot{J}_2\rho - J_2\dot{\rho}\right)\left(\cos k\,\hat{\sigma}_y - \sin k\,\hat{\sigma}_x\right)\Big], \tag{8}$$

where $\hat{\sigma}_j$ are the Pauli matrices in the basis of the degenerate eigenstates defined by Eqs. (4) and (5). Following Ref. 28, we can express the displacement of the state $|\psi^{\alpha}_{n_0}(0)\rangle$ as

$$\Delta x = \sum_{\nu\mu} c^*_\nu c_\mu D^{\alpha}_{\mu\nu}, \tag{9}$$

where the displacement matrix D^{α}_{ab} can be recast as

$$D^{\alpha}_{\mu\nu} = \frac{1}{2\pi}\int_0^T dt \int_{-\pi}^{\pi} dk \left[W^{\dagger}_{\alpha} F^{\alpha}_{kt} W_{\alpha}\right]_{\mu\nu}, \tag{10}$$

with $\alpha = \pm$, $F^{\alpha}_{kt} = \partial_k\Gamma^{\alpha}_t - \partial_t\Gamma^{\alpha}_k + i[\Gamma^{\alpha}_t, \Gamma^{\alpha}_k]$ denoting the non-Abelian field strength matrix and $\Gamma^{\pm}_k$ indicating the k-connection $[\Gamma^{\pm}_k]_{\nu\nu'} = \langle\psi^{\pm}_{\nu}(k)|i\partial_k|\psi^{\pm}_{\nu'}(k)\rangle$. Equations (9) and (10) illustrate the topological and geometrical significance of non-Abelian Thouless pumping. In these regards, a particularly intriguing aspect of this phenomenon, rooted in its geometric nature, is the exceptional level of control it offers over both the state's evolution and the transport process. By suitably designing the pumping cycles, we can indeed engineer different combination of translations along the lattice and rotation in the degenerate subspace. The general structure of the transformations generated by different cycles can be analyzed using Eq. (8). For instance, this equation reveals that variations in J_1 and ρ, while keeping $J_2 = 0$, result in rotations around σ_y. Similarly, setting $\rho = 0$ leads to rotations around σ_z and $J_1 = 0$ leads to rotations around a k-dependent combination of σ_x and σ_y. Consequently, cycles confined to the hyperplanes $J_1 = 0$, $J_2 = 0$, or $\rho = 0$ commute with one another. Therefore, designing geometric evolutions with non-commutative properties requires these parameters to differ from zero over a finite time interval along the cycle.

In the construction of the pumping cycles, we impose two conditions: (i) $\min_{k,t}|E_+(k) - E_-(k)|T \gg 1$, and (ii) $\max_{k,t}|\partial_k E_{\pm}(k)|T \ll a$, with a denoting the lattice spacing. Condition (i) relates the driving period T with the band-gap, and it expresses the adiabaticity criterion. Instead, condition (ii) relates T with the group velocity of a band, and it requires that the displacement generated by the pumping in one cycle, typically of the order of one unit cell, is much smaller than the dynamically induced dispersion (see the supplementary material and Refs. 47 and 48 for details). In flat band systems,[28] condition (ii) is always fulfilled as $\partial_k E_{\pm}(k) = 0$. Conversely, when the bands are not flat, satisfying simultaneously both inequalities guarantees that the pumping is *adiabatic* and *weakly dispersive*. As discussed in the supplementary material, there exist a wide region in the parameter space where both conditions (i) and (ii) are satisfied. This region is within the reach of current cold atoms experiments on Thouless pumping (see the supplementary material for details).

IV. PROTOCOLS AND QUANTUM STATE PROPAGATION

We consider two pumping cycles, called C_1 and C_2. As common starting point of these cycles at $t = 0$, we choose $J_1 = J_2 = \mu = 0$ and $\rho = \rho_0 \neq 0$. This choice reduces the ladder in Fig. 1(a) to a set of decoupled dimers, as only the transversal hopping is present. As prescribed by Eqs. (4) and (5), we initialize the system in a Wannier state $|\psi^{\pm}_{n_0}(0)\rangle$ localized in the unit-cell n_0 belonging to the $\pm$ bands. We set: $|v^{\pm}_{a,n_0}\rangle = \frac{\delta_{n,n_0}}{\sqrt{2}}[|a_{n,U}\rangle \pm |a_{n,D}\rangle]$ and $|v^{\pm}_{b,n_0}\rangle = \frac{\delta_{n,n_0}}{\sqrt{2}}[|b_{n,U}\rangle \mp |b_{n,D}\rangle]$.

The cycles C_1 and C_2 are schematically depicted in Figs. 1(b) and 1(c). During both cycles, J_1 and ρ change adiabatically. However, in cycle C_1, the on-site potential remains zero, while J_2 varies adiabatically. Conversely, in cycle C_2, J_2 is set to zero, and μ undergoes a variation. The Wilson loops $W^{\pm}$ entering the adiabatic evolution operator defined in Eqs. (7) and (8) can be calculated analytically using the Wilczek–Zee connection and, up to phase factors, lead to (see the supplementary material for details)

$$W^{\pm}_{C_1} = \begin{pmatrix} e^{ik} & 0 \\ 0 & e^{-ik} \end{pmatrix} \quad W^{\pm}_{C_2} = \begin{pmatrix} 0 & 1 \\ -1 & 0 \end{pmatrix}. \tag{11}$$

Replacing Eq. (11) in Eq. (6), we obtain that, over one period T cycle, C_1 shifts the states of one unit-cell to their right/left, respectively—i.e., the excitations $|v^{\pm}_{a,n_0}\rangle$ and $|v^{\pm}_{b,n_0}\rangle$ are shifted to $v^{\pm}_{a,n_0+1}$ and $v^{\pm}_{b,n_0-1}$, respectively, i.e., the cycles C_1 generates chiral quantized change displacement along the ladder, as shown in Fig. 2. Cycle C_2 on the other hand swaps these state within one unit-cell—i.e., the excitations $|v^{\pm}_{a,n_0}\rangle$ and $|v^{\pm}_{b,n_0}\rangle$ are mapped to $|v^{\pm}_{b,n_0}\rangle$ and $-|v^{\pm}_{a,n_0}\rangle$, respectively (see the supplementary material for details).

The numerical results in Figs. 1(e)–1(p), obtained by solving numerically the Schrödinger equation $i\partial_t|\psi\rangle = H(t)|\psi\rangle$, are in agreement with the analytical prediction obtained in Eqs. (6), (8), and (11). The symmetries $E_- = -E_+$ of the Bloch bands allow us to focus on the positive band E_+ and show results only for the states $|v^{+}_{a,n_0}\rangle$ and $|v^{+}_{b,n_0}\rangle$. Along both C_1 and C_2, the conditions (i) and (ii) reduce simply to $\frac{1}{2\rho_0} \ll T$ since the weak dispersion conditions is automatically fulfilled along these cycles. In our numerical tests, we set $\rho_0 \cdot T = 50$ consistently with the experiments carried out, e.g., in an atomic quantum gas microscope[49–52] (see the supplementary material for details). Figures 1(g) and 1(n), respectively, show the initially states $|v^{+}_{a,n_0}\rangle$ and $|v^{+}_{b,n_0}\rangle$. Their propagation along the cycle C_1 are shown in Figs. 1(f) and 1(m) and their final state in Figs. 1(e) and 1(l). Likewise, the propagation of $|v^{+}_{a,n_0}\rangle$ and $|v^{+}_{b,n_0}\rangle$ along one period of cycle C_2 are shown in Figs. 1(h) and 1(o), and the correspondent final state in Figs. 1(i) and 1(p). Focusing at first on the time evolution along cycle C_1—i.e., Figs. 1(f) and 1(m)—we notice that in the first half of the cycle, namely $0 \leq t \leq \frac{T}{2}$, where only the hoppings J_1 and ρ are activated, $|v^{+}_{a,n_0}\rangle$ and $|v^{+}_{b,n_0}\rangle$ are shifted within the unit-cell. Then, in the second half of the

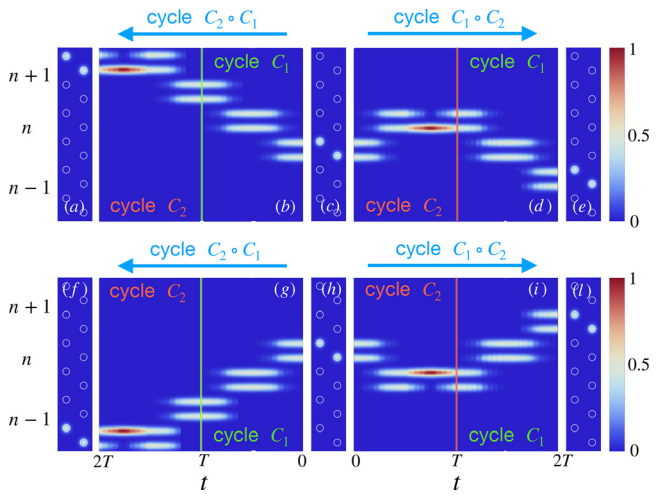

FIG. 2. (a)–(e) Numerically evaluated field's intensity along $C_2 \circ C_1$ and $C_1 \circ C_2$ starting from state $|v^+_{a,n_0}\rangle$. (c) shows the initial excited $|v^+_{a,n_0}\rangle$. (b) and (d) show the evolution according to $C_2 \circ C_1$ and $C_1 \circ C_2$, respectively. (a) and (e) show the field intensity in the final states after one pumping cycles $C_2 \circ C_1$ and $C_1 \circ C_2$. (f)–(l) Same as (d)–(h) with initial condition $|v^+_{b,n_0}\rangle$.

cycle, namely, $\frac{T}{2} \leq t \leq T$, where only the hoppings J_2 and ρ are activated, $|v^+_{a,n_0}\rangle$ and $|v^+_{b,n_0}\rangle$ are shifted to the neighboring unit-cell. For cycle C_2—i.e., Figs. 1(h) and 1(o), in the first half of the cycle, where only J_1 and ρ are activated, $|v^+_{a,n_0}\rangle$ and $|v^+_{b,n_0}\rangle$ are shifted within the unit-cell. Then, in the second half of the cycle, where only the hopping ρ and the potential μ are activated, the states $|v^+_{a,n_0}\rangle$ and $|v^+_{b,n_0}\rangle$ are rotated.

These two cycles therefore yield different chiral quantized displacement, as in C_1 we set $\mu(t) \equiv 0$ to avoid state rotation, while in C_2, we set $J_2(t) \equiv 0$ to prevent transport along the chains. Furthermore, they allow to demonstrate the non-Abelian nature of the Thouless pumping since their holonomies do not commute, i.e., $C_2 \circ C_1 \neq C_1 \circ C_2$. This is shown in Fig. 2 for the initial states $|v^+_{a,n_0}\rangle$ and $|v^+_{b,n_0}\rangle$. Following $C_2 \circ C_1$, the states $|v^+_{a,n_0}\rangle$ and $|v^+_{b,n_0}\rangle$ are first shifted to their neighboring unit-cells in opposite directions and then swapped. In the opposite case $C_1 \circ C_2$, the states are first swapped and then shifted to the neighboring unit cells. The final states in the two cases are different and they are shown in Figs. 2(a) and 2(f) and Figs. 2(e) and 2(l).

V. MAPPING ONTO A YANG MONOPOLE MODEL

To further elucidate the topology and the physics of the ladder Hamiltonian given in Eq. (1), it is useful to note that it can be mapped onto a spinful Rice–Mele Hamiltonian with staggered magnetic field. To this end, we perform a local unitary transformation $\mathscr{U}$ and redefine the chain in terms of spin $\sigma = \uparrow, \downarrow$ and pseudo-spin coordinates $\tau = a, b$—namely, we set

$$a^\dagger_{k,\uparrow} = \frac{e^{-i\frac{\pi}{4}}a^\dagger_{k,U} + e^{i\frac{\pi}{4}}a^\dagger_{k,D}}{\sqrt{2}} \quad a^\dagger_{k,\downarrow} = \frac{-e^{-i\frac{\pi}{4}}a^\dagger_{k,U} + e^{i\frac{\pi}{4}}a^\dagger_{k,D}}{\sqrt{2}}$$
$$b^\dagger_{k,\uparrow} = \frac{e^{-i\frac{\pi}{4}}b^\dagger_{k,U} + e^{+i\frac{\pi}{4}}b^\dagger_{k,D}}{\sqrt{2}} \quad b^\dagger_{k,\downarrow} = \frac{e^{-i\frac{\pi}{4}}b^\dagger_{k,U} - e^{+i\frac{\pi}{4}}b^\dagger_{k,D}}{\sqrt{2}}. \tag{12}$$

The Hamiltonian written in terms of the spinor creation and annihilation operators $a^\dagger_k = (a^\dagger_{k,\uparrow}, a^\dagger_{k,\downarrow})$ and $b^\dagger_k = (b^\dagger_{k,\uparrow}, b^\dagger_{k,\downarrow})$ reads

$$H = \sum_k \big[(-J_k\, a^\dagger_k \sigma_y b_k + \text{H.c.}) + a^\dagger_k(\mathbf{B}_a \cdot \vec{\sigma})\, a_k + b^\dagger_k(\mathbf{B}_b \cdot \vec{\sigma})\, b_k\big] \tag{13}$$

with $\mathbf{B}_a = (0, -\mu, \rho)$ and $\mathbf{B}_b = (0, \mu, \rho)$. This system is visualized in Fig. 3(a), where the pseudo-spin components $\tau = a, b$ are shown with red and blue circles, respectively, and in it, the spin degrees of freedom $\sigma = \uparrow, \downarrow$ are represented with the white arrows.

We now consider the effect of the cycles C_1 and C_2 in the new coordinates. At $t = 0$, the Hamiltonian given in Eq. (13) is proportional to σ_z and the initial states are localized on a or b sites with spin $\uparrow$ or $\downarrow$ spin, for example, $|v^+_{a,n_0}\rangle \to |a_{n_0,\uparrow}\rangle$ and $|v^-_{a,n_0}\rangle \to |a_{n_0,\downarrow}\rangle$. We look at the evolution of these states by tracing the total density matrix $\hat{\rho}$ over the spatial and spin indices, respectively, n and σ, $\hat{\rho}_\tau = \text{Tr}_{n,\sigma}\hat{\rho}$. This reduced density matrix is then decomposed via the Pauli matrices to evaluate the expectation values of the pseudospin vector $\langle\tau_i\rangle = \text{Tr}[\hat{\rho}_\tau \tau_i]$. Its three components are vector plotted in Figs. 3(b) and 3(c), where we show the evolution of $|a_{n_0,\uparrow}\rangle$ along cycles C_1 and C_2. We note that at certain points along the cycles, the Bloch vector representing the pseudospin density matrix has a vanishing length indicating a state with maximally entangled spin and pseudospin. Finally, we remark that the spinful Rice–Mele model of Eq. (13) can be related to the $SO(5)$ mean-field theory describing BCS and spin-density-wave (SDW) quasi-particles proposed in Ref. 37, the role of the latter being played by pseudospin excitations. The non-Abelian holonomy characterizing the Hamiltonian in Eq. (13) can be therefore related to a Yang monopole singularity. This is analogous to what happens for the Zhang–Demler Hamiltonian[37] and experimentally studied in Ref. 53. Specifically, Eq. (13) can be recast in terms of $\Phi^\dagger_k = (a^\dagger_{k,\uparrow}, a^\dagger_{k,\downarrow}, b^\dagger_{k,\uparrow}, b^\dagger_{k,\downarrow})$ to describe an $SO(5)$ spinor Hamiltonian $H_M = \sum_k \Phi^\dagger_k [Q_\mu \hat{\Gamma}_\mu] \Phi_k$ with $\hat{\Gamma}_\mu$ denoting Dirac Γ-matrices introduced in Ref. 37, i.e., $\hat{\Gamma}_1 = i\tau_y \otimes \sigma_x$, $\hat{\Gamma}_2 = i\tau_y \otimes \sigma_y$, $\hat{\Gamma}_3 = i\tau_y \otimes \sigma_z$, $\hat{\Gamma}_4 = \tau_0 \otimes \sigma_z$, and $\hat{\Gamma}_5 = \tau_0 \otimes \sigma_x$ and $\mathbf{Q} = \{iJ_x, iJ_y, i\mu, \rho, 0\}$ (see the supplementary material for details). Note that in $\mathbf{Q}$ the component corresponding to $\hat{\Gamma}_5$ vanishes and it can be activated by, e.g., turning

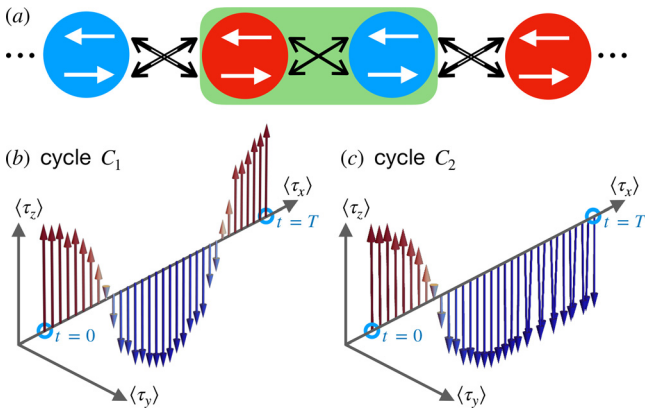

FIG. 3. (a) Schematic representation of the spin Hamiltonian H in Eq. (13) where the green box indicates a unit-cell. The red and blue circles represent the pseudo-spin components a_n and b_n, respectively, object of the fields $\mathbf{B}_a$ and $\mathbf{B}_b$. (b) Rotation of the pseudo-spin $\tau = a$ and $\tau = b$ represented with upward red arrow and downward blue arrow, respectively, for the initial state $|v^+_{a,n_0}\rangle$ along cycles C_1. (c) Same as (b) for cycle C_2.

into a complex variable the staggered interchain hopping $\rho \to \rho_1 + i\rho_2$ in Eq. (1).

VI. CONCLUSIONS

In conclusion, we have demonstrated how to realize non-Abelian Thouless pumping in a Rice–Mele ladder with time-dependent couplings. The model we propose exhibits doubly degenerate Bloch bands, and it has both fundamental and practical significance.

First, it enables an exceptional degree of control over transport. By appropriately combining different pumping cycles, the proposed non-Abelian pumping protocol can (i) generate arbitrary lattice translations and (ii) provide a route to implement all single-particle gates within the degenerate subspace. This result holds potential for quantum computing and metrology, extending beyond the expectation values of observables and significantly enhancing the capabilities of standard holonomic gates.[40,41] To understand this point, it is useful to consider Eq. (8). This equation describes the various holonomic transformations that can be achieved by adiabatically manipulating the system parameters. In particular, some of these transformations depend on k, making their effects non-local. This happens in particular for the cycle C_1, which produces a conditional shift of the degenerate states. The answer to this question is thus twofold. On the one hand, Eq. (8) illustrates how to generate all single-particle gates in k-space, and on the other hand, it demonstrates that generating local single-particle gates requires composing different k-dependent transformations or enlarging the parameter space, e.g., allowing the parameter ρ to be complex. By doing so, it is easy to construct holonomic cycles yielding rotation around two orthogonal axes, therefore enabling the construction of all single-qubit gates.

Second, the Rice–Mele ladder systems discussed in this work can be implemented not only in photonic setup[29] but also using cold atoms in optical lattices[54] or quantum gas microscopy.[49,55–57] It may thus pave the way to the first experimental realization of non-Abelian Thouless pumping in a quantum many-body systems—analogously to the Abelian Thouless pumping of interacting quantum particles in Rice–Mele chains.[14–18]

The experimental implementation of the model has to take into account the effect of fluctuations and inaccuracies in the manipulation of the lattice parameters. Nevertheless, highly accurate recent experimental implementations, see, for example, Ref. 29, suggest that extremely robust non-Abelian Thouless pumping can be generated also in the presence of disorder and inaccuracies. Furthermore, theoretical and numerical evidence of this robustness has been presented in Ref. 28. There, it was shown that there are different regimes of non-Abelian Thouless pumping with disorder, depending on the ratio between disorder strength and driving period. It emerged that in the worst case, i.e., when the strength of disorder is comparable with the inverse of the driving period, disorder affects the structure of the transformation but does not generate dispersion.

Third, we show that the Rice–Mele ladder can be related to an $SO(5)$ spinor model for Yang monopoles, hinting at a possible strategy to use Thouless pumps to investigate the dynamics of high-energy and strongly correlated systems. Furthermore, it enables the investigation of higher-order topological systems as discussed in Ref. 53.

SUPPLEMENTARY MATERIAL

See the supplementary material to detail the calculation of the Bloch eigenstates; detail the calculation of the holonomies $\Gamma_t^{\pm}$; detail the conditions for adiabatic and weakly dispersive pumping; detail the calculation of the Wilson loops and the one period evolution of cycles C_1 and C_2; and detail the mapping of the ladder to an $SO(5)$ model.

ACKNOWLEDGMENTS

The authors acknowledge inspiring discussions with Monika Aidelsburger and Immanuel Bloch. V.B. and R.C. acknowledge financial support from PNRR MUR Project No. PE0000023-NQSTI financed by the European Union—Next Generation EU. This work was co-funded by European Union—PON Ricerca e Innovazione 2014-2020 FESR/FSC—Project No. ARS01 _00734 QUANCOM and PNRR MUR Project No. CN 00000013-ICSC.

AUTHOR DECLARATIONS

Conflict of Interest

The authors have no conflicts to disclose.

Author Contributions

Carlo Danieli: Formal analysis (equal); Investigation (equal); Methodology (equal); Validation (equal); Writing – original draft (equal). **Valentina Brosco:** Conceptualization (equal); Formal analysis (equal); Investigation (equal); Methodology (equal); Supervision (equal); Validation (equal); Writing – original draft (equal). **Laura Pilozzi:** Formal analysis (equal); Investigation (equal); Methodology (equal); Validation (equal); Writing – original draft (equal). **Roberta Citro:** Conceptualization (equal); Formal analysis (equal); Investigation (equal); Methodology (equal); Supervision (equal); Validation (equal); Writing – original draft (equal).

DATA AVAILABILITY

The data that support the findings of this study are available from the corresponding author upon reasonable request.

REFERENCES

[1]M. V. Berry, Proc. R. Soc. London, Ser. A **392**, 45 (1984).
[2]F. Wilczek and A. Zee, Phys. Rev. Lett. **52**, 2111 (1984).
[3]F. Wilczek and A. Shapere, *Geometric Phases in Physics* (World Scientific, Singapore, 1989).
[4]D. J. Thouless, M. Kohmoto, M. P. Nightingale, and M. den Nijs, Phys. Rev. Lett. **49**, 405 (1982).
[5]S. Murakami, N. Nagosa, and S.-C. Zhang, Phys. Rev. B **69**, 235206 (2004).
[6]X.-L. Qi and S.-C. Zhang, Rev. Mod. Phys. **83**, 1057 (2011).
[7]D. J. Thouless, Phys. Rev. B **27**, 6083 (1983).
[8]R. Citro and M. Aidelsburger, Nat. Rev. Phys. **5**, 87 (2023).
[9]M. Lohse, C. Schweizer, O. Zilberberg, M. Aidelsburger, and I. Bloch, Nat. Phys. **12**, 350 (2016).
[10]S. Nakajima, T. Tomita, S. Taie, T. Ichinose, H. Ozawa, L. Wang, M. Troyer, and Y. Takahashi, Nat. Phys. **12**, 296 (2016).
[11]C. Schweizer, M. Lohse, R. Citro, and I. Bloch, Phys. Rev. Lett. **117**, 170405 (2016).
[12]Y. E. Kraus, Y. Lahini, Z. Ringel, M. Verbin, and O. Zilberberg, Phys. Rev. Lett. **109**, 106402 (2012).
[13]L. Stenzel, A. L. C. Hayward, U. Schollwöck, and F. Heidrich-Meisner, Phys. Rev. A **102**, 023315 (2020).
[14]Y. Ke, X. Qin, Y. S. Kivshar, and C. Lee, Phys. Rev. A **95**, 063630 (2017).
[15]M. Nakagawa, T. Yoshida, R. Peters, and N. Kawakami, Phys. Rev. B **98**, 115147 (2018).

[16]W. Liu, S. Hu, L. Zhang, Y. Ke, and C. Lee, Phys. Rev. Res. **5**, 013020 (2023).
[17]A.-S. Walter, Z. Zhu, M. Gächter, J. Minguzzi, S. Roschinski, K. Sandholzer, K. Viebahn, and T. Esslinger, Nat. Phys. **19**, 1471 (2023).
[18]K. Viebahn, A.-S. Walter, E. Bertok, Z. Zhu, M. Gächter, A. A. Aligia, F. Heidrich-Meisner, and T. Esslinger, Phys. Rev. X **14**, 021049 (2024).
[19]A. Cerjan, M. Wang, S. Huang, K. P. Chen, and M. C. Rechtsman, Light Sci. Appl. **9**, 178 (2020).
[20]S. Huang, Y.-Q. Zhu, and Z. Li, Phys. Rev. A **109**, 052213 (2024).
[21]N. Mostaan, F. Grusdt, and N. Goldman, Nat. Commun. **13**, 5997 (2022).
[22]P. S. Jung, M. Parto, G. G. Pyrialakos, H. Nasari, K. Rutkowska, M. Trippenbach, M. Khajavikhan, W. Krolikowski, and D. N. Christodoulides, Phys. Rev. A **105**, 013513 (2022).
[23]S. Ravets, N. Pernet, N. Mostaan, N. Goldman, and J. Bloch, "Thouless pumping in a driven-dissipative Kerr resonator array," arXiv:2407.02627 (2024).
[24]M. Jürgensen, S. Mukherjee, C. Jörg, and M. C. Rechtsman, Nat. Phys. **19**, 420 (2023).
[25]P. Marra, R. Citro, and C. Ortix, Phys. Rev. B **91**, 125411 (2015).
[26]P. Marra and R. Citro, Eur. Phys. J. Spec. Top. **226**, 2781 (2017).
[27]L. Taddia, E. Cornfeld, D. Rossini, L. Mazza, E. Sela, and R. Fazio, Phys. Rev. Lett. **118**, 230402 (2017).
[28]V. Brosco, L. Pilozzi, R. Fazio, and C. Conti, Phys. Rev. A **103**, 063518 (2021).
[29]Y.-K. Sun, X.-L. Zhang, F. Yu, Z.-N. Tian, Q.-D. Chen, and H.-B. Sun, Nat. Phys. **18**, 1080 (2022).
[30]L. Pilozzi and V. Brosco, Nat. Phys. **18**, 968 (2022).
[31]O. You, S. Liang, B. Xie, W. Gao, W. Ye, J. Zhu, and S. Zhang, Phys. Rev. Lett. **128**, 244302 (2022).
[32]V. Brosco, L. Pilozzi, and C. Conti, Phys. Rev. B **104**, 024306 (2021).
[33]L.-M. Duan, Science **292**, 1695 (2001).
[34]L. Faoro, J. Siewert, and R. Fazio, Phys. Rev. Lett. **90**, 028301 (2003).
[35]V. Brosco, R. Fazio, F. W. J. Hekking, and A. Joye, Phys. Rev. Lett. **100**, 027002 (2008).
[36]V. Neef, J. Pinske, F. Klauck, L. Teuber, M. Kremer, M. Ehrhardt, M. Heinrich, S. Scheel, and A. Szameit, Nat. Phys. **19**, 30 (2023).
[37]E. Demler and S.-C. Zhang, Ann. Phys. **271**, 83 (1999).
[38]C. N. Yang and R. L. Mills, Phys. Rev. **96**, 191 (1954).
[39]C. N. Yang, J. Math. Phys. **19**, 320 (1978).
[40]P. Zanardi and M. Rasetti, Phys. Lett. A **264**, 94 (1999).
[41]J. Zhang, T. H. Kyaw, S. Filipp, L.-C. Kwek, E. Sjöqvist, and D. Tong, Phys. Rep. **1027**, 1 (2023).
[42]A. Bottarelli, M. Frigerio, and M. G. A. Paris, AVS Quantum Sci. **5**, 025001 (2023).
[43]K. von Klitzing, Nat. Phys. **13**, 198 (2017).
[44]B. Jeckelmann and F. Piquemal, Ann. Phys. **531**, 1800389 (2019).
[45]M. Yu, X. Li, Y. Chu, B. Mera, F. N. Ünal, P. Yang, Y. Liu, N. Goldman, and J. Cai, Natl. Sci. Rev. **11**, nwae065 (2024).
[46]M. J. Rice and E. J. Mele, Phys. Rev. Lett. **49**, 1455 (1982).
[47]S. Hu, Y. Ke, Y. Deng, and C. Lee, Phys. Rev. B **100**, 064302 (2019).
[48]W. Liu, Y. Ke, and C. Lee, "Shortcuts to adiabatic thouless pumping," arXiv:2401.17081 [quant-ph] (2024).
[49]A. Impertro, S. Karch, J. F. Wienand, S. Huh, C. Schweizer, I. Bloch, and M. Aidelsburger, Phys. Rev. Lett. **133**, 063401 (2024).
[50]A. Impertro, J. F. Wienand, S. Häfele, H. von Raven, S. Hubele, T. Klostermann, C. R. Cabrera, I. Bloch, and M. Aidelsburger, Commun. Phys. **6**, 166 (2023).
[51]C. Braun, R. Saint-Jalm, A. Hesse, J. Arceri, I. Bloch, and M. Aidelsburger, Nat. Phys. **20**, 1306 (2024).
[52]A. Impertro, S. Huh, S. Karch, J. F. Wienand, I. Bloch, and M. Aidelsburger, "Realization of strongly-interacting meissner phases in large bosonic flux ladders," arXiv:2412.09481 (2024).
[53]S. Sugawa, F. Salces-Carcoba, A. R. Perry, Y. Yue, and I. B. Spielman, Science **360**, 1429 (2018).
[54]M. Atala, M. Aidelsburger, M. Lohse, J. T. Barreiro, B. Paredes, and I. Bloch, Nat. Phys. **10**, 588 (2014).
[55]W. S. Bakr, J. I. Gillen, A. Peng, S. Folling, and M. Greiner, Nature **462**, 74 (2009).
[56]J. F. Sherson, C. Weitenberg, M. Endres, M. Cheneau, I. Bloch, and S. Kuhr, Nature **467**, 68 (2010).
[57]C. Gross and W. S. Bakr, Nat. Phys. **17**, 1316 (2021).